THESIS FOR THE DEGREE OF LICENTIATE OF ENGINEERING

Terahertz sensing for non-destructive characterisation of pharmaceutical tablets

ANIS MORADIKOUCHI

CHALMERS
UNIVERSITY OF TECHNOLOGY

Terahertz and Millimetre Wave Laboratory
Department of Microtechnology and Nanoscience-MC2
Chalmers University of Technology
Gothenburg, Sweden, 2022

Terahertz sensing for non-destructive characterisation of pharmaceutical tablets

ANIS MORADIKOUCHI

ORCID: 0000-0003-3811-1024

Technical Report No. MC2-447
ISSN 1652-0769
This thesis has been prepared using LaTeX.

Chalmers University of Technology
Department of Microtechnology and Nanoscience-MC2
Terahertz and Millimetre Wave Laboratory
SE-412 96 Gothenburg, Sweden
Phone: +46 (0)31 772 1000
www.chalmers.se

Printed by Chalmers Reproservice
Gothenburg, Sweden, March 2022

To my family.

Abstract

The pharmaceutical industry is shifting from conventional batch manufacturing to continuous manufacturing. To realise continuous manufacturing, it is crucial to assess the product quality of tablets at different stages of the production line. Therefore, there is a high need for quality control methods that are fast, non-destructive, and compact, with the possibility of implementation in the production line for real-time measurements. However, traditional quality control methods are typically slow and destructive. In our work, we propose the terahertz frequency domain (THz-FD) technique, based on all-electronic solutions, as a fast, sensitive, and non-destructive sensing technique with miniaturization capabilities for a future compact sensing system. In this technique, the effective refractive index of tablets at the terahertz frequency range is extracted from the transmission measurements of the scattering parameters of the tablets using a vector network analyser. Then, the effective refractive index is transferred to tablet density by using an empirical model and later is translated to tablet porosity. The measurement results show that the THz-FD technique could differentiate tablets with different refractive index and detect and quantify the minute changes of tablet density and porosity with the variation of design parameters. The design parameters were compaction force during tableting process, the concentration of the ingredients, and the particle size of the ingredients. It was observed that in our study the compaction force and filler particle size had the major impact on tablet porosity. In conclusion, it was demonstrated that the THz-FD technique based on electronic solutions allows for fast, sensitive, and non-destructive measurements of pharmaceutical tablets that open for compact instrument systems capable of in-line sensing in the tablet manufacturing process.

Keywords: Terahertz technology, frequency domain, non-destructive, dielectric characterisation, porosity measurements, pharmaceutical tablets, sensing.

List of publications

This thesis is based on the following appended publications:

[A] **Anis Moradikouchi**, Martin Lindsjö, Jan Stake, Staffan Folestad, Helena Rodilla, “Non-Destructive Characterization of Pharmaceutical Tablets Using Terahertz Frequency Domain Spectroscopy,” in proceedings of the *44th International Conference on Infrared, Millimeter, and Terahertz Waves (IRMMW-THz)*, Paris, 2019, pp. 1–2, doi: 10.1109/IRMMW-THz.2019.8874004.

[B] **Anis Moradikouchi**, Anders Sparén, Staffan Folestad, Jan Stake, Helena Rodilla, “Small Variation of Active Pharmaceutical Ingredient Concentration Can Be Observed with THz Frequency Domain Spectroscopy,” in proceedings of the *46th International Conference on Infrared, Millimeter, and Terahertz Waves (IRMMW-THz)*, Chengdu, 2021, pp. 1, doi: 10.1109/IRMMW-THz50926.2021.9567162.

[C] **Anis Moradikouchi**, Anders Sparén, Staffan Folestad, Jan Stake, Helena Rodilla, "Terahertz Frequency Domain Sensing for Fast Porosity Measurement of Pharmaceutical Tablets," in *International journal of pharmaceutics*, 2022, doi: 10.1016/j.ijpharm.2022.121579.

Acknowledgments

First and foremost, I would like to thank my main supervisor, Helena Rodilla, for the guidance, support, energy, encouragement, and fruitful discussions that I've had with her. Secondly, I would like to thank my co-supervisor Jan Stake, for his support, encouragement, constructive feedback, and all I learnt about writing and publishing. My big thanks to Anders Sparén, apart from being my great supervisor in the industry, I thank him for his support, encouragement, and kind heart. Many thanks to Staffan Folestad for his supervision on my project and the fruitful discussions that we had. Also, thanks to Mats Myremark for his help and creativity with the fabrication part of my measurement set-up in the shortest possible time. A big thanks to my dear office mates, Juan, Divya, Peter, Marlene, who I feel very lucky to have them for the scientific discussions, companionship, support, and warm vibes. The same goes for the rest of my TML former and present colleagues (Xinxin, Mohammed Asad, Junjie, Yin, Vladmir, Sergey, Thomas, Andrei, etc). I would like to give big thanks to my beloved mother, father, brothers, Mojtaba, Mostafa, Morteza, and my sister, Najmeh, who always believed in me and supported me; I am who I am because of them. And big thanks to my dear friends (Mahtab, Lida, Mehrnaz, Atefeh, Zeynab, Salimeh, Amir, Reza, and Arman), whose presence and support warmed my heart through my PhD journey.

This work was supported by the Swedish foundation for strategic research (SSF), ID17-0011, and by AstraZeneca, PTD # 570, Gothenburg, Sweden.

Acronyms

NIR:	Near infrared
THz-TDS:	Terahertz time-domain spectroscopy
THz-FD:	Terahertz frequency-domain
VNA:	Vector network analyzer
API:	Active pharmaceutical ingredients
MCC:	Microcrystallyne cellulose
SOLT:	Short, Open, Load, Through
SEM:	Scanning electron microscopy
TEM:	Transverse electromagnetic

Mathematical symbols

c	Speed of light in vacuum
F	Compaction force
f	Porosity
f_{THz}	THz Porosity
g	Shape factor
j	Imaginary unit, $\sqrt{-1}$
k_0	Wavenumber in vacuum
$\hat{n}$	Complex refractive index
n_s	Real refractive index
S_{ij}	S-parameter from port j to port i
T	Complex transmission coefficient
V	Voltage
w	Concentration of the ingredients
Z	Wave impedance
Γ	Reflection coefficient
δ	Loss tangent
$\hat{\epsilon}$	Complex dielectric permittivity
ϵ'	Real part of dielectric permittivity
ϵ''	Imaginary part of dielectric permittivity
ϵ_{eff}	Effective permittivity
κ_s	Imaginary part of refractive index
λ	Wavelength
λ_0	Wavelength in vacuum
l	Tablet thickness
ϕ	Phase of transmission
ρ_{tablet}	Tablet density
ρ_{true}	True density
$\rho_{tab,THz}$	THz tablet density
τ	time delay

Contents

CHAPTER 1

Introduction

1.1 Introduction

In the pharmaceutical industry, tablets are one of the most convenient dosage forms for the administration of drugs to patients. Tablets are bulk assemblies of solids in the form of particles, and gases in the form of air voids. A typical tablet formulation consists of active pharmaceutical ingredient(s) (API) and excipients with different functionalities, like fillers, binders, and lubricants. It is the properties of each constituent and the interactions between them that define the tablet properties, such as density, porosity, friability, elasticity, and plasticity [1]. The assessment of tablet properties during tablet manufacturing processes is essential to ensure that the final product fulfils the required specifications.

Recently, the pharma industry is shifting from a conventional batch manufacturing system to continuous manufacturing. The advantages of continuous manufacturing include improved product quality by a constant quality control process, efficiency in productivity and production costs, ensuring sustainability by waste reduction, and space-saving by having the production process compacted in one site [2]. To realise continuous manufacturing, there is a

need to develop quality control methods, which are fast and non-destructive, with the possibility of implementation in the production line for real-time measurements [3].

Tablet density and porosity are physical tablet properties that play a crucial role in the disintegration and dissolution of tablets [4]. Although various techniques for inspecting these properties have been developed over the past years, there are no in-line sensing techniques, and off-line techniques are typically slow and destructive. One commonly used technique is mercury porosimetry [5] that is a reliable but destructive technique with negative environmental impact. X-ray microtomography [6] is a non-destructive technique with the disadvantage of using ionizing radiation and being slow. Near-infrared spectroscopy is a non-destructive and fast technique, but suffers from scattering effect and low penetration depth through samples due to short wavelength [7]. Gas in Scattering Media Absorption Spectroscopy (GASMAS) [8]–[10] is a non-destructive at-line technique to measure optical porosity. Additionally, the microwave frequency range is also attractive for material characterisation because of their high penetration depth, but with the drawback of large beam diameter compared with the diameter of the tablets. Terahertz (THz) spectroscopy has recently emerged as a fast, non-destructive tool for pharmaceutical applications [11], such as to estimate the physical properties of tablets like refractive index and porosity [12]. The THz spectral range is defined between 100 GHz (3 mm) to 10 THz (30 μm), which is between the millimetre and the far-infrared region of the electromagnetic spectrum. The longer wavelength of THz waves compared to the techniques mentioned above tackles the challenges like short penetration depth and scattering effects and permits to extract the information that represents the bulk properties of tablets [7]. Dielectric characterisation of tablets using terahertz time-domain spectroscopy (THz-TDS) has recently been explored for porosity measurements [12]. Juuti et al. used a THz spectrometer to study the correlation between the effective refractive index and tablet porosity [13]. Bawuah et al. used THz-TDS to obtain the porosity of tablets composed of one excipient [14] and later tablets consisting of several excipients and an API [3]. Naftaly et al. proposed the use of THz-TDS to analyse the open porosity and scattering loss of powder compacts [15]. Skelbæk-Pedersen et al. used THz-TDS to study tablet porosity and particle fragmentation during tableting [16]. Stanzinger et al. demonstrated a lab-experimental THz-TDS set-up for monitoring powder flow densification [17].

THz-TDS instrumentation is a versatile tool for dielectric characterisation in a lab environment. However, the miniaturisation of the THz-TDS system for implementation in the production line still remains a challenge.

In this thesis, the THz-FD technique, based on all-electronic solutions, is proposed as a fast, sensitive, and non-destructive sensing technique with the miniaturisation capabilities required for a future compact measurement system for in-line sensing [18]–[21]. In our technique, we obtain the tablet density and porosity based on the effective refractive index of tablets at the terahertz frequency range [22]. We extracted the effective refractive index of the tablets from the transmission measurement of the scattering parameters of the tablets, using a vector network analyser and quasi-optical components. In order to extract porosity, an empirical linear relation between effective refractive index and tablet density was used. The results showed that the THz-FD technique could differentiate tablets with different dielectric constants. We also observed that THz measurements were highly sensitive to the minute changes of tablet density and porosity due to varying the design factors, like the particle size the of filler and the API, the compaction force, and the API concentration. Therefore, the THz-FD technique based on electronic solutions allows for fast, non-destructive measurement systems with the possibility of implementation in the production line for real-time measurements.

CHAPTER 2

Background

This chapter describes the basic concepts for density and porosity measurement of pharmaceutical tablets. Section 2.1 explains the concept of porosity. Section 2.2 presents the currently in-use porosity measurement techniques, and 2.3 presents THz spectroscopy as an emerging technique for porosity measurements. Tablets can be considered as an effective medium, and tablet porosity can be extracted from the effective refractive index of the tablets by the measurement of the scattering parameters of tablets. We study the concepts of scattering parameters in section 2.4, propagation of waves in a medium in section 2.5, and effective medium approximation in section 2.6, propagation of waves in three-layer medium in section 2.7.

2.1 Porosity in pharmaceutics

Pharmaceutical tablets are porous entities consisting of APIs, excipients, and air voids (pores). Particle size, shape, and location can influence tablets porosity, see Fig. 2.1. Apart from the specification of the excipients and API, porosity can have a significant effect on the performance of the tablets [1]. Porosity influences the penetration rate of the solvents into the tablet matrix,

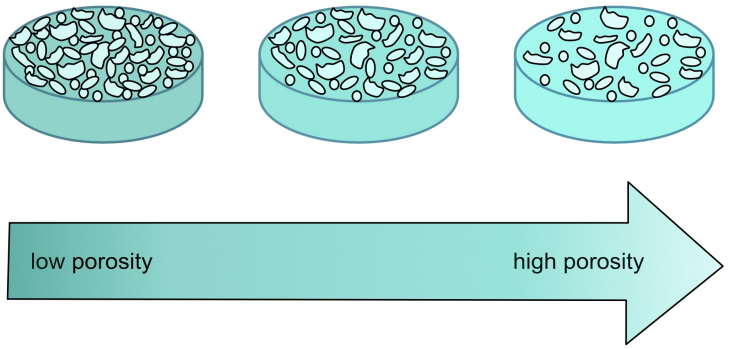

Figure 2.1: The size, shape, and location of particles can influence tablets' porosity.

which affects tablets disintegration, dissolution, and bioavailability [23], [24].

2.2 Porosity measurement techniques

Various approaches for studying porosity have been investigated like mercury porosimetry, X-ray computed microtomography, Near infrared spectroscopy, and terahertz spectroscopy, which will be explained below.

- **Mercury porosimetry:** This technique uses a pressurised chamber to force mercury into the voids in the porous tablet. The pore size distribution and pore volume of void spaces can be determined by the penetration of mercury into the tablet. The amount of pressure required to intrude mercury into the pores is inversely proportional to the size of the pores. Volume and pore size distributions can be obtained from the applied pressure and the data generated by the Mercury porosimetry instrument using the Washburn equation [5]. However, this measurement technique is slow (1-3 hours) and destructive, and hazardous for health and environment.

- **X-ray microtomography:** This technique is a non-destructive technique based on the interaction of electromagnetic waves in the X-ray region with matter and is advantageous for pore structure analysis. Several studies investigated the density distribution inside tablets [25] and

ribbons [26],an intermediate state in drug manufacturing, and orosity and pore structure [6]. Drawbacks include ionizing radiation, which is hazardous to human operators over time, and long measurement time. Besides that, pores smaller than the resolution cannot be detected, and increasing the resolution demands large processing memory and storage space [6].

- **Near Infrared Spectroscopy:** This technique measures the interaction of electromagnetic waves in the near infrared (NIR) region with matter. It is based on the molecular vibrations, overtones, and combinations of vibration bands that occur in the material in the NIR region. It has been used to measure the physical properties of tablets, including blend uniformity [27] and ribbon porosity characterisation [28], [29]. This method is non-destructive, can be performed rapidly without the need for sample preparation, and can be implemented in the manufacturing process for real-time measurements. However, the molecular overtone and combination bands seen in the NIR region are typically broad and have limited selectivty, often requiring multivariate calibration techniques to extract the desired information. Moreover, due to relatively short wavelengths compared to the particle size of powders used in the tablet formulation, the NIR technique suffers from scattering effect and low penetration depth through samples that restricts the extracted information to the surface properties of tablets [7].

  Other techniques like powder pycnometry [30] and GASMAS [8]–[10] have been applied for porosity measurements. Despite the reliable results, powder pycnometry is a slow and destructive technique, and GASMAS is suitable for at-line measurements.

2.3 Terahertz spectroscopy for tablet characterisation

Terahertz spectroscopy has recently emerged as a fast non-destructive tool for tablet characterisation that tackles the mentioned limitations like scattering effects, short penetration depth, and complex nature of the measured spectra and the need for multivariate calibration techniques. The terahertz (THz) spectral region is defined in the range of 100 GHz (3 mm) to 10 THz

(30 μm), which is between the millimetre and the far infrared region of the electromagnetic spectrum. The longer wavelength of THz waves comparing to the techniques mentioned above provides longer penetration depth and lower scattering effects. This permits to probe tablets and extract information that represent bulk properties of materials [7]. Additionally, the low photon ionisation energy of THz radiation makes it a safe sensing method.

2.3.1 THz time-domain spectroscopy

Terahertz time-domain spectroscopy (THz-TDS) is based on the interaction of short THz pulses with matter. This technique measures both the amplitude and phase information of the transmitted signal through the sample. An ultra-fast laser sends optical pulses with femtosecond pulse duration into a photoconductive antenna to be transformed into a picosecond THz pulse. Usually, the pulse is guided and focused on the sample via off-axis parabolic mirrors. The THz pulse interacts with the sample under test and is collected at the detector together with the beam from the delay line [7], see Fig. 2.2. This technique has the advantages of a wide frequency bandwidth from 100

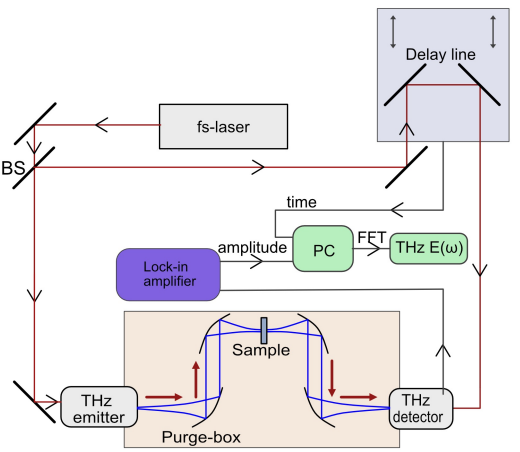

Figure 2.2: Schematic of a THz time-domain set-up. The red lines show the laser beam from the fs laser to the detector, the blue lines show the THz beam, and the black lines illustrate signal connections to a lock-in amplifier and a computer

GHz to 2 THz, with the downside of being a bulky measurement setup that needs careful alignment of the optical components [31].

2.3.2 THz frequency-domain spectroscopy

THz frequency-domain spectroscopy (THz-FDS) is based on the interaction of continuous electromagnetic waves with matter. One approach for THz-FDS is electronic solutions based on heterodyne transmitters and receivers [32]. A vector network analyser is a key instrument in THz-FD technique for measuring the scattering parameters of materials, which will be explained in Sec. 2.4. In this method, a vector network analyser (VNA) along with two frequency extenders, two horn antennas, and four off-axis parabolic mirrors (if needed, in order to focus the beam on the sample), see Fig. 2.3, are used to emit continuous electromagnetic waves to a sample and measure the scattering parameters of the sample, both phase and amplitude of the reflection and transmission coefficients. The VNA generates sinusoidal continuous waves, which are up-converted to the THz range by the frequency extenders [32]. The first horn antenna after the frequency extender transmits the generated THz signal, which is then guided and focused on the sample by two off-axis parabolic mirrors. After probing the sample, the signal is guided by the other two off-axis parabolic mirrors to the second horn antenna. The signal is down-converted to the low frequencies by the second frequency extender and is transferred to the VNA. The advantages of this technique are high frequency resolution, high dynamic range [33], high SNR, and the possibility of set-up miniaturisation. The downside is that the measurement bandwidth is restricted to the bandwidth of rectangular waveguides before horn antennas, which can be used for the frequencies up to 1.5 THz at the moment.

2.4 Scattering parameters

Direct measurements of a network usually require the measurement of the magnitude and phase of a transmitted wave into the network and the reflected wave from the device. Scattering parameters represent the relation between the transmitted and reflected waves. Scattering matrix allows a device to be treated as a black box and provides a complete description of the device by modeling it as an n-port network and relating the voltage waves reflected from

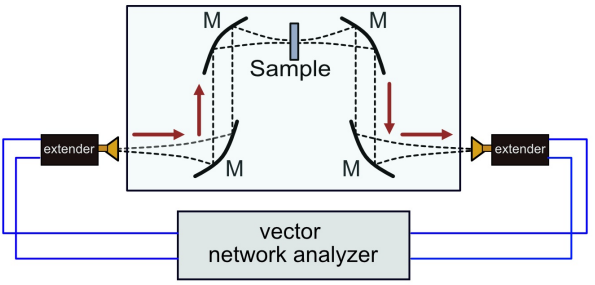

Figure 2.3: Schematic of a THz frequency-domain measurement set-up, consisting of a VNA, frequency extenders, and quasi-optical components.

the ports to those incident on the ports, as in:

$$S_{ij} = \left.\frac{V_i^-}{V_j^+}\right|_{V_{k\neq j}^+=0}, \tag{2.1}$$

where V_i^- is the voltage reflected from port i and V_j^+ is the voltage incident to the port j, while other ports are terminated with a matched load. As depicted in Fig. 2.4, for a two port network we have:

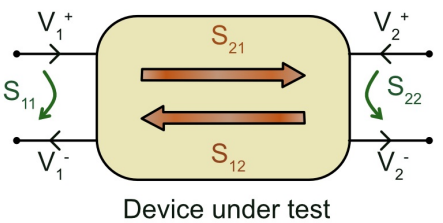

Figure 2.4: Illustration of the scattering parameters of a two-port network.

$$\begin{bmatrix} V_1^- \\ V_2^- \end{bmatrix} = \begin{bmatrix} S_{11} & S_{12} \\ S_{21} & S_{22} \end{bmatrix} \begin{bmatrix} V_1^+ \\ V_2^+ \end{bmatrix}, \tag{2.2}$$

If the two-port device is symmetric, we have:

$$S_{11} = S_{22}, \tag{2.3}$$

where S_{11} is the reflection coefficient at port 1, Γ_1, while port 2 is terminated with a matched load. S_{22} is the reflection coefficient at port 2, Γ_2, while port 1 is terminated with a matched load.

If the two-port device is reciprocal, meaning there is no active devices, ferrites, or plasmas in the network, we have:

$$S_{12} = S_{21}. \tag{2.4}$$

where S_{12} is the transmission coefficient, T, from port 2 to port 1, while port 1 is terminated with a matched load.

If the network is lossless, we have the condition below for the scattering matrix:

$$\sum_{k=1}^{2} S_{ki} S_{kj}^{*} = \delta_{ij}, \text{ for all i, j,} \tag{2.5}$$

where $\delta_{ij} = 1$ if $i = j$, and $\delta_{ij} = 0$ if $i \neq j$ [34], [35].

2.5 Propagation of electromagnetic waves in a medium

The refractive index of a medium, $\hat{n}_s$, is a number that describes the behaviour of a propagating electromagnetic wave through the medium. It is the ratio of the velocity of light in vacuum to its velocity in the medium. Refractive index is a complex number with real and imaginary parts, $\hat{n}_s = n_s - j\kappa_s$. The real part, n_s, indicates the phase velocity, while the imaginary part, κ_s, indicates attenuation when the electromagnetic wave propagates through the material.

The permittivity of a medium is a measure of the electric polarisability of the medium when subjected to an external electric field. The electric field causes the polarisation of the atoms or molecules of the material to create electric dipole moments. A material with high permittivity polarises more and create larger dipole moment in the direction of electric field. The real part of permittivity describes the material's ability to interact with the electric

field without absorbing energy, while the imaginary part shows the material's ability to permanently absorb energy.

The real and imaginary part of the permittivity can be obtained from the complex refractive index as in equation 2.6:

$$\begin{aligned} \hat{\epsilon}_r &= \epsilon'_r - j\epsilon''_r = \hat{n}_s^2, \\ \epsilon'_r &= n_s^2 - \kappa_s^2, \\ \epsilon''_r &= 2n_s\kappa_s. \end{aligned} \tag{2.6}$$

For a material with negligible conductivity, the ratio of the imaginary to the real part of the permittivity is called loss tangent, as in:

$$tan\ \delta = \frac{\epsilon''}{\epsilon'}. \tag{2.7}$$

2.6 Effective medium approximation

An effective medium is a medium consisting of different constituents, which their size is small compared to the wavelength of the propagating electromagnetic wave. This medium can be considered as a homogeneous medium with an effective permittivity ϵ_{eff}. In this thesis, we consider pharmaceutical tablets an effective medium consisting of solid particles and air voids (pores). The permittivity of the tablet can be modeled by an electrical circuit using capacitors in series and parallel to represent the randomly oriented particles and air voids, see Fig. 2.5. Different approximations have been developed to characterise effective mediums, like Maxwell Garnett [36] and Bruggeman models [37]. In these two models, the particle size of inclusions is small compared to the wavelength, thus the scattering effects are assumed negligible. The prior knowledge of the absolute permittivity, volume fraction, and the shape factor of the constituents are needed to obtain the effective permittivity of the medium.

2.6.1 Maxwell Garnett model

The Maxwell Garnett model considers a host medium, the matrix, with embedded inclusions. It is valid for mediums with low volume fractions of embedded inclusions, and it considers the particles' shape of inclusions spherical.

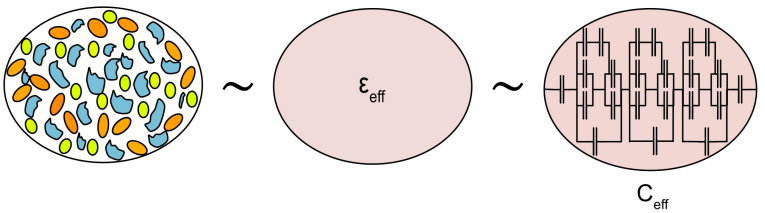

Figure 2.5: A medium consisting of different constituents can be considered as an homogeneous medium with an effective permittivity ϵ_{eff}
. The electrical circuit equivalent to the effective medium is a combination of series and parallel capacitors.

The effective permittivity, ϵ_{eff}, of the medium can be computed as in:

$$(\frac{\epsilon_{eff} - \epsilon_m}{\epsilon_{eff} + 2\epsilon_m}) = f_i(\frac{\epsilon_i - \epsilon_m}{\epsilon_i + 2\epsilon_m}), \tag{2.8}$$

where ϵ_i is the permittivity of the inclusions, ϵ_m of the matrix, and f_i is the volume fraction of the inclusions.

2.6.2 Bruggeman model

The Bruggeman model considers the host medium and embedded inclusions equally important and all constituents are inclusions embedded in an effective medium. The general form of the Bruggeman model can be expressed as:

$$\sum_{i=0}^{i} f_i \frac{\epsilon_i - \epsilon_{eff}}{\epsilon_{eff} + g(\epsilon_j - \epsilon_{eff})} = 0. \tag{2.9}$$

For a two phase medium consisting of air and solid, the Bruggeman model can be expressed as:

$$\frac{\epsilon_{solid} - \epsilon_{eff}}{\epsilon_{eff} + g(\epsilon_{solid} - \epsilon_{eff})}(1 - f) + \frac{\epsilon_{air} - \epsilon_{eff}}{\epsilon_{eff} + g(\epsilon_{air} - \epsilon_{eff})} f = 0. \tag{2.10}$$

where ϵ_{solid} and ϵ_{air} are the permittivity of the solid phase and air voids, respectively, f is the volume fraction of the air, and g is the shape factor of the constituents.

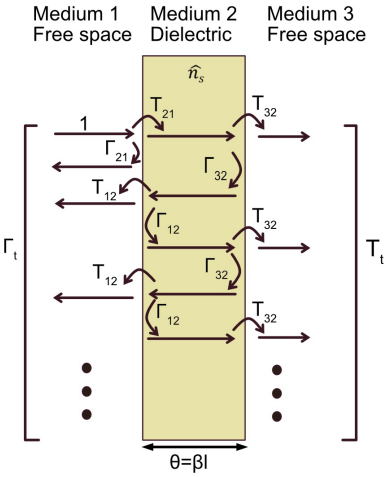

Figure 2.6: Partial reflections and transmissions on a three-layer medium.

2.7 Electromagnetic wave propagation in three-layer medium

We can model the propagation of an electromagnetic wave through a three-layer medium by using the theory of small reflections [34]. In Fig. 2.6, we assume TEM plane waves travel from medium 1 to medium 3 with a normal angle of incidence. Medium 1 and 3 are free space, and medium 2 is filled by a dielectric with refractive index $\hat{n}_s$ and thickness t. The dielectric is homogeneous and has flat surfaces.

The total transmission from medium 1 to 3, T_t, can be obtained as an infinite sum of partial reflections and transmissions, as in:

$$T_t = T_{21}T_{32}e^{-j\theta} + T_{21}T_{32}\Gamma_{23}\Gamma_{21}e^{-j3\theta} + T_{21}T_{32}\Gamma_{23}^2\Gamma_{21}^2e^{-j5\theta} + ..., \quad (2.11)$$

where T_{mn} is the transmission coefficient from medium n to m, and Γ_{mn} is the reflection coefficient from medium n to m. The partial reflection and transmission coefficients can be computed as below:

$$\Gamma_{21} = \frac{Z_2 - Z_0}{Z_2 + Z_0} = \frac{\frac{Z_0}{\hat{n}_s} - Z_0}{\frac{Z_0}{\hat{n}_s} + Z_0} = \frac{1 - \hat{n}_s}{1 + \hat{n}_s}, \tag{2.12}$$

where Z_0 is the impedance of free space, Z_2 is the impedance of the dielectric.

$$\Gamma_{21} = -\Gamma_{12} = -\Gamma_{32} = \Gamma, \tag{2.13}$$

$$T_{21} = 1 + \Gamma_{21}, \tag{2.14}$$

$$T_{32} = 1 + \Gamma_{32}, \tag{2.15}$$

Thus, T_t can be expressed as in:

$$T_t = (1 + \Gamma)(1 - \Gamma)e^{-j\theta}(1 + \Gamma^2 e^{-j2\theta} + \Gamma^4 e^{-j4\theta} + ...), \tag{2.16}$$

$$T_t = (1 - \Gamma^2)e^{-j\theta} \sum_{i=0}^{\infty} (\Gamma^2 e^{-j2\theta})^i, \tag{2.17}$$

using the summation of the geometric series

$$\sum_{i=0}^{\infty} x^i = \frac{1}{1 - x}, \text{ for } |x| < 1 \tag{2.18}$$

we can express equation 2.17 as in:

$$T_t = \frac{(1 - \Gamma^2)e^{-j\theta}}{1 - \Gamma^2 e^{-j2\theta}}, \tag{2.19}$$

and if the refractive index of the dielectric is close to 1, then $|\Gamma|^2$ is ≈ 0, so we can approximate:

$$T_t \approx e^{-j\theta}. \tag{2.20}$$

Following the same procedure as for total transmission coefficient, the total reflection from medium 1 to 3, Γ_t, can be obtained as an infinite sum of partial reflections and transmissions [34], as in:

$$\begin{aligned}\Gamma_t &= \Gamma_{21} + \Gamma_{32}T_{21}T_{12}e^{-j2\theta} + \Gamma_{32}^2\Gamma_{12}T_{21}T_{12}e^{-j4\theta} + ... \\ &= \Gamma\frac{1-e^{-j2\theta}}{1-\Gamma^2e^{-j2\theta}},\end{aligned} \tag{2.21}$$

and if the refractive index of the dielectric is close to 1, then $|\Gamma|^2$ is ≈ 0, so we can approximate:

$$\Gamma_t \approx \Gamma(1-e^{-j2\theta}). \tag{2.22}$$

CHAPTER 3

Tablet preparation

This chapter describes the tablet sets used in this work. Different sets of training tablets with two different formulations were used. The first formulation, explained in section 3.1, consisted of only excipients, and tablets were produced by a tablet press. These tablets were used to investigate the sensitivity of terahertz waves to tablets with different dielectric constants and compaction forces. The second formulation, explained in 3.2, consisted of API and excipients. These tablets were used to investigate the sensitivity of the terahertz waves to the variations of the design factors such as the API concentration, compaction force, particle size of powders.

3.1 First formulation

Three sets of training tablets, with seven tablets in each set were produced. The tablet press Kilian S 300 (Romaco Kilian, Cologne, Germany) was used to produce the training sets of tablets. Using a tablet press, it is possible to adjust and control the mass and the compaction force applied to the powder compact in the tableting process, which results in tablets with different densities. This is achieved by making use of the adjustable lower and upper punches in the

tablet press. The lower punch was used to adjust the mass of the tablets and the higher punch was used to tune the compaction force applied on the tablets. This directly affects the height, density and porosity of the tablets.

The tablets were flat faced and round with a diameter of 20 mm. The tablets' height was measured several days after compaction to allow for the mechanical relaxation. In each set, the mass of the tablets was kept constant, while different compaction forces were applied. As a result, tablets with different thickness and densities were produced. For a constant mass, thicker tablets have lower density and higher porosity.

Chemicals components of tablets

Three training tablet sets with different dielectric constants were produced. Set 1 was made of Microcrystallyne cellulose, set 2 of Succinic acid, and set 3 of Benzophenone. In each tablet set, there were seven tablets with different compaction forces.

A. Microcrystallyne cellulose

Microcrystallyne cellulose (MCC) is a conventional pharmaceutical excipient used as a filler with advantages like tabletability, compatibility and being suitable for direct compaction [38]. The characteristics of set 1 can be found in table 3.1. As can be seen, the height of the tablets decreases with increasing the compaction force. This causes the tablet density to increase and the tablet porosity to decrease.

Table 3.1: Data of tablet set 1, MCC.

Sample number	Height (mm)	Tablet density (gcm^{-1})	Compaction force (kN)
1	3.464	0.276	22.3
2	3.326	0.287	25.5
3	3.234	0.295	28.9
4	3.163	0.302	31.2
5	3.125	0.306	33.5
6	3.052	0.313	38.1
7	2.967	0.322	48.3

B. Succinic acid

Succinic acid is a common organic acid, which is used in different industries as a precursor to produce chemicals such as solvents, perfumes, lacquers, plasticizer, dyes, and photographic chemicals [39]. The characteristics of tablet set 2 can be found in table 3.2. The same trend explained in table 3.1 follows here.

Table 3.2: Data of tablet set 2, Succinic acid.

Sample number	Height (mm)	Tablet density (gcm^{-1})	Compaction force (kN)
1	3.066	0.312	10.6
2	3.015	0.317	13.2
3	2.944	0.324	16.9
4	2.913	0.328	18.5
5	2.823	0.338	29.5
6	2.795	0.342	31.9
7	2.763	0.346	38.7

Table 3.3: Data of tablet set 3, Benzophenone.

Sample number	Height (mm)	Tablet density (gcm^{-1})	Compaction force (kN)
1	2.913	0.232	4.0
2	2.809	0.241	6.4
3	2.717	0.249	9.8
4	2.650	0.255	14.3
5	2.600	0.260	16.7
6	2.583	0.262	20.1
7	2.532	0.267	24.5

C. Benzophenone

Benzophenone is used as a flavour ingredient, fragrance enhancer, and as an additive for plastics, coatings and adhesive formulations, and to prevent ultraviolet light-induced damage to cosmetics [40]. The characteristics of tablet

set 3 can be found in table 3.3. The same trend explained in table 3.1 follows here.

3.2 Second formulation

We studied a sample set of 69 tablets consisting of API, Ibuprofen, excipient, Mannitol, and lubricant, Magnesium stearate. A full factorial design of the API particle size at two levels of ($d_{50} \sim 71$, 154 μm) and the excipient particle size at two levels of ($d_{50} \sim 91$, 450 μm) were set, where the d_{50}-value is the median diameter of the particle size distribution found at 50% in the cumulative distribution. This design was repeated at five API concentration levels ($\sim$ 16, 18, 20, 22, and 24 w/w %), and Magnesium stearate concentration was kept $\sim$ 1 w/w% for all tablets. Details about the design of experiments can be found in table 3.4, where experiments 21–23 are center points that are used in the evaluation of the design to estimate the experimental precision. Tablets from all powder blends were manufactured at three compaction forces ($\sim$ 8, 12, and 16 kN), resulting in 69 different tablets. Information about the tablets parameters are given in table 3.5. All tablets were flat faced, with a nominal weight of 300 mg, a diameter of 10.0 mm and a thickness in the range of 2.9–3.4 mm.

Chemicals components of tablets

A. Ibuprofen

Ibuprofen is a drug substance widely used for treating pain, fever, and inflammation [41]. Ibuprofen particles are needle-shaped with low flowability [42].

B. Mannitol

Mannitol is a widely used filler in the formulation of chewable or rapidly disintegrating tablet formulations. It is water soluble, nonhygroscopic, produces a semisweet taste, and has good compactibility [43].

C. Magnesium stearate

Magnesium stearate is widely used as a lubricant for pharmaceutical tableting; it is relatively inexpensive, provides high lubrication with a high melting point

and chemical stability [44].

Table 3.4: Design of experiments for the tablets. Design factors are API particle size at two levels (71, 154 μm) , excipient particle size at two levels (91, 450 μm), API concentration at five levels (16, 18, 20, 22, 25 w/w%) and compaction force at three levels (8, 12, 16 kN) (not included in the table).

Experiment number	API particle size d_{50} (μm)	filler particle size d_{50} (μm)	API concentration (w/w%)
1	71	91	16
2	154	91	16
3	71	450	16
4	154	450	16
5	71	91	18
6	154	91	18
7	71	450	18
8	154	450	18
9	71	91	20
10	154	91	20
11	71	450	20
12	154	450	20
13	71	91	22
14	154	91	22
15	71	450	22
16	154	450	22
17	71	91	24
18	154	91	24
19	71	450	24
20	154	450	24
21	95	211	20
22	95	211	20
23	95	211	20

Table 3.5: List of characterised tablets in this study. The ingredients were Ibuprofen supplied by IOL Chemicals and Pharmaceuticals (Punjab, India), Mannitol Parteck M100 and Mannitol Parteck M200 from Merck KGaA (Darmstadt, Germany), Mannitol Pearlitol 400DC from Roquette (Lestrem, France), magnesium stearate from AstraZeneca R&D (Södertälje, Sweden) . The thickness of each tablet was measured five times by a micrometer. Tablet density was calculated from the weight and dimensions of tablets, and true density of compact powder was calculated using equation 7.

Tablet	Thickness (mm)	Mass (mg)	Tablet density (g cm$^-$3)	True density (g cm$^-$3)	API con. (w/w %)	Com. force (kN)
Set 1						
1	3.340	306	1.166	1.433	16.8	7.4
	3.190	306	1.221		16.8	12.2
	3.106	306	1.254		16.8	16.0
2	3.325	304	1.164	1.436	16.2	7.9
	3.175	304	1.219		16.2	12.1
	3.089	304	1.253		16.2	15.9
3	3.072	303	1.256	1.432	16.0	8.0
	2.976	303	1.296		16.0	11.8
	2.926	303	1.318		16.0	15.8
4	3.095	305	1.255	1.431	16.2	8.4
	3.015	305	1.288		16.2	11.9
	2.956	305	1.314		16.2	15.9
Set 2						
5	3.298	303	1.170	1.425	18.5	8.2
	3.174	303	1.216		18.5	12.2
	3.076	303	1.254		18.5	15.8
6	3.356	306	1.161	1.427	18.0	7.9
	3.203	306	1.216		18.0	12.0
	3.121	306	1.248		18.0	15.9
7	3.123	306	1.248	1.421	18.4	8.2
	3.029	306	1.286		18.4	12.1
	2.961	306	1.316		18.4	15.8
8	3.117	307	1.254	1.424	17.9	8.5
	3.057	307	1.278		17.9	11.9
	3.014	307	1.297		17.9	15.3
Set 3						
9	3.321	304	1.165	1.416	20.6	8.2
	3.180	304	1.217		20.6	12.2
	3.103	304	1.247		20.6	16.0
10	3.371	307	1.160	1.419	19.9	7.8
	3.250	307	1.203		19.9	11.7
	3.146	307	1.242		19.9	15.4
11	3.066	302	1.254	1.417	19.5	8.0
	2.985	302	1.288		19.5	11.9
	2.972	302	1.294		19.5	15.2
12	3.144	306	1.239	1.418	19.3	8.4
	3.054	306	1.276		19.3	12.0
	3.008	306	1.295		19.3	16.0

Tablet	Thickness (mm)	Mass (mg)	Tablet density (g cm^{-}3)	True density (g cm^{-}3)	API con. (w/w %)	Com. force (kN)
Set 4						
13	3.335	304	1.161	1.407	22.7	8.3
	3.195	304	1.212		22.7	11.9
	3.133	304	1.236		22.7	16.1
14	3.336	304	1.160	1.409	22.2	8.3
	3.230	304	1.198		22.2	11.8
	3.129	304	1.237		22.2	15.6
15	3.124	303	1.235	1.402	22.9	7.9
	3.012	303	1.281		22.9	13.0
	2.973	303	1.298		22.9	16.0
16	3.154	305	1.231	1.408	21.4	7.9
	3.071	305	1.264		21.4	11.7
	3.041	305	1.277		21.4	14.6
Set 5						
17	3.348	304	1.156	1.398	24.8	7.8
	3.215	304	1.204		24.8	11.8
	3.151	304	1.228		24.8	15.5
18	3.375	307	1.158	1.401	24.1	8.0
	3.270	307	1.195		24.1	11.5
	3.154	307	1.239		24.1	15.8
19	3.142	304	1.232	1.393	25.0	7.8
	3.050	304	1.296		25.0	12.1
	3.021	304	1.281		25.0	15.6
20	3.148	305	1.234	1.398	23.8	8.5
	3.064	305	1.267		23.8	12.3
	3.036	305	1.279		23.8	16.0
21	3.372	309	1.167	1.419	20.0	8.7
	3.240	309	1.214		20.0	12.3
	3.164	309	1.244		20.0	16.1
22	3.378	307	1.157	1.418	20.1	8.3
	3.241	307	1.206		20.1	11.8
	3.107	307	1.258		20.1	16.7
23	3.378	305	1.149	1.417	20.4	7.9
	3.204	305	1.212		20.4	12.0
	3.097	305	1.254		20.4	15.9

CHAPTER 4

Terahertz characterisation of tablets

This chapter describes the employed measurement set-ups for measuring the tablets (section 4.1), and the analytical methods for the extraction of effective refractive index (section 4.2) and porosity (section 4.3).

4.1 Measurement setup

We have used free space frequency-domain measurements in transmission mode to characterise the tablets. Free space measurement is contact-less, non-destructive and doesn't require sample preparation.

Our first set-up consisted of a VNA (Keysight PNA-X), frequency extenders, and horn antennas. The Gaussian beam after the horn antenna expands as it is traveling in the free space and due to the large diameter of the beam reaching the surface of the tablet, this set-up is suitable for tablets with a large diameter. We used this set-up for the tablets with the first formulation with the diameter of 20 mm. However, it is possible to manipulate the beam by employing parabolic mirrors. Adding two off-axis parabolic mirrors to the setup collimates the beam, and adding four mirrors collimates and focuses the beam to the sample. In the second measurement set-up four off-axis parabolic

mirrors were added to the set-up to facilitate the measurements of tablets with smaller diameters, tablets with second formulation, with the cost of being more bulky. In our measurements, the empty holder was used as a reference for relative measurements between the tablets and air. Relative measurements suppress the uncertainty due to possible misalignment of components, loss in the optical path, and temperature and humidity variation.

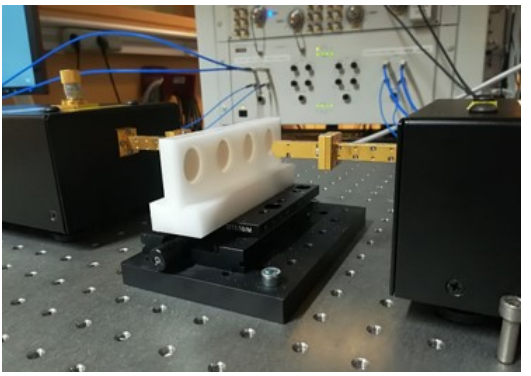

Figure 4.1: Photograph of experimental set-up in transmission mode for scattering parameters measurements.

4.1.1 First measurement set-up and procedure

The frequency range 325-500 GHz, VDI frequency extenders 570 WM, was selected to avoid scattering effects (long wavelength compared to the particle size) and maintain small beam diameter. The VNA was calibrated at the interface between the waveguide flanges of the extenders and the horn antennas using the SOLT (Short, Open, Load, Through) calibration method. The sample holder was placed at the far field distance between the two antennas, see Fig. 4.1. The estimated beam diameter at the surface of the sample was approximately 10 mm. Each tablet was measured four times to verify the repeatability of the measurements. Before tablet measurement, the empty sample holder was measured as a reference for relative measurements [Paper A].

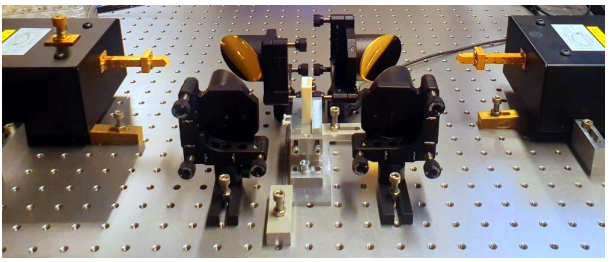

(a)

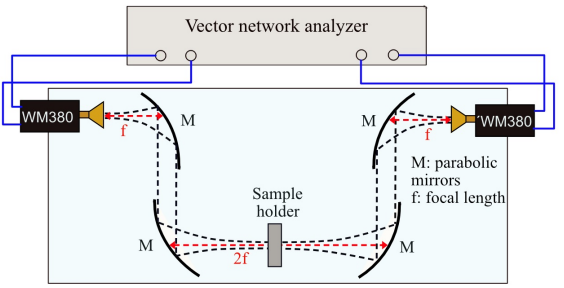

(b)

Figure 4.2: a) Photograph and b) schematics of the experimental set-up showing THz S-parameter measurements in transmission mode. The blue square represents the area showed in the photograph.

4.1.2 Second measurement set-up and procedure

The frequency range was selected at the range of 500-750 GHz, VDI frequency extenders WM380, to ensure a small beam size compared to the tablets diameter and to avoid absorption peaks, as Ibuprofen has an absorption peak around 1 THz. During measurements, the intermediate frequency bandwidth was set to 1 kHz, and number of frequency points were set to 251. In order to visualise and help with the alignment of the quasi-optical set-up, the vector network analyser was calibrated at the interface between the waveguide flanges of the extenders and the horn antennas using the SOLT (Short, Open, Load, Through) calibration method. The focal length of the mirrors was 76.4 mm, and the horn antennas and sample holder were placed at the focal point. The estimated beam diameter at the focal point is approximately 2 mm, which is the beam waist of the Gaussian beam at the phase center of the horn antenna. Each frequency sweep took less than one second to complete. Each tablet was measured ten times in consecutive frequency sweeps to verify the measurement repeatability. Before each tablet measurement, the empty sample holder was measured as a reference for relative measurements [Paper B and C].

4.2 Effective refractive index extraction

The complex effective refractive index of the tablets can be extracted from a relative measurements of the complex transmission coefficients ($T = S_{21}$) between sample and air. In this thesis, we used two different methods for the extraction of the effective refractive index. The first method, multiple reflections, considers the small reflections of THz waves inside the tablet. The second method, one-path transmission, simplifies the extraction of $\hat{n}_s$ by not considering the small reflections and is suitable for low-loss mediums.

The effective refractive index is assumed to be homogeneous across the tablets, and the electromagnetic wave at the surface of the tablets is assumed to be a plane wave with a normal angle of incidence. In this work, we only focus on the real part for characterising the tablet density and porosity. The imaginary part can be used for other purposes like studying the moisture content.

4.2.1 Multiple reflections:

In this method, $\hat{n}_s$ can be extracted from the comparison of the measured relative transmission coefficients with a modeled one [45]. The relative transmission between sample and air, T_s/T_a, can be modeled as in equation 4.1 [46]:

$$\left(\frac{T_s}{T_a}\right)_m = \frac{(1-\Gamma_1^2)}{1-\Gamma_1^2 e^{-2jk_0\hat{n}_s l}} e^{-jk_0 l(\hat{n}_s-1)}, \tag{4.1}$$

where the total transmission, T_t in the Fig. 4.3, has been used to consider

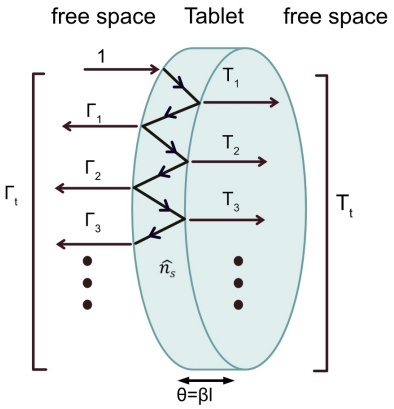

Figure 4.3: Partial transmissions and reflections inside a tablet.

the multiple reflections inside the tablet. k_0 is the free space wave number, and l is the thickness of the tablet. Γ_1 is the complex reflection coefficient in the interface between air and tablet, as in:

$$\Gamma_1 = \frac{1-\hat{n}_s}{1+\hat{n}_s}. \tag{4.2}$$

The value of $\hat{n}_s$ versus frequency was obtained numerically by solving equation 4.3:

$$f(\hat{n}_s) = \left(\frac{T_s}{T_a}\right)_m - \left(\frac{T_s}{T_a}\right)_d = 0. \tag{4.3}$$

This equation has multiple possible solutions because of the periodic nature of the exponential terms. To find the correct solution, $n_{s,i}$ from the equation

below was used as an initial estimate:

$$n_{s,i} = 1 + \frac{\tau c}{2\pi l}, \tag{4.4}$$

where c is the speed of light in vacuum and τ is the time delay, $\tau = -\frac{\Delta\phi}{\Delta\omega}$, which is the slope of the phase of measured relative transmission versus frequency [47], [48]. In order to verify the results, the model, $(T_s/T_a)_m$, was recalculated using the obtained $\hat{n}_s$, and its magnitude and phase were compared with the measurement data, $(T_s/T_a)_d$ [Paper C].

4.2.2 One-path transmission:

In this method, we neglect the multiple reflections of waves inside the tablets. The imaginary part, κ_s, can be extracted from the amplitude of the relative transmission, which will not be discussed here. The real part of $\hat{n}_s$, n_s, can be obtained from the phase shift of the relative transmission, using the first transmission path, T_1, in the Fig. 4.3 as in [49]:

$$n_s = 1 - \frac{(\Delta\phi - 2m\pi)\lambda}{2\pi l}, \tag{4.5}$$

where $\Delta\phi = \phi - \phi_0$ is the relative phase shift of the transmission coefficient between sample and empty holder, l is the tablet thickness, and m is the number of wavelength inside tablets. It accounts for the possible phase ambiguity, which can be caused due to the multiple wavelengths inside thick tablets (compared to the wavelength of THz waves). The phase ambiguity can be addressed by approximating the number of the wavelength, as in:

$$(n_{s,0} - 1)\frac{l}{\lambda_0} - \frac{1}{2} < m < (n_{s,0} - 1)\frac{l}{\lambda_0} + \frac{1}{2}, \tag{4.6}$$

where λ_0 is the wavelength in free space, $n_{s,0}$ is the initial guess for n_s.

This method is simple, but neglects the multiple reflections inside the tablets and requires an initial guess for n_s to calculate m [Paper A].

4.3 Porosity extraction

In this section, we explain the extraction of tablet porosity from effective refractive index measurements. Porosity, f, can be calculated using equation 4.7 [50]:

$$f = 1 - \frac{\rho_{tablet}}{\rho_{true}}, \tag{4.7}$$

where ρ_{tablet} is the density of the tablet and ρ_{true} is the true density of the powder blend.

Tablet density can be measured manually by measuring the weight and volume of tablet, but is time consuming and not suitable for real time measurements. In order to address this, tablet density can be obtained from the effective refractive index of tablets. Given that the tablet density varies in a small range, a linear relation between effective refractive index of tablets and tablet density can be assumed [22]. Therefore, tablet density can be obtained by the fast measurement of the effective refractive index, and it can be translated to porosity using equations 4.8 - 4.9:

$$\rho_{tab,THz} = \rho_1 n_s + \rho_0, \tag{4.8}$$

$$f_{THz} = 1 - \frac{\rho_{tab,THz}}{\rho_{true}}, \tag{4.9}$$

where $\rho_{tab,THz}$ and f_{THz} are the tablet density and porosity obtained from terahertz measurements, respectively.

In order to obtain the coefficients, ρ_1 and ρ_0, the tablet density obtained from mechanically measurement of mass and volume of the samples can be used for calibration.

ρ_{true} in equation 4.7 can be calculated from the concentration, w_i, and the true density of the constituents, $\rho_{true,i}$, from literature and their data sheet, as in [50] [Paper C]:

$$\frac{1}{\rho_{true}} = \sum_{i=1}^{3} \frac{w_i}{\rho_{true,i}}. \tag{4.10}$$

CHAPTER 5

Results

This chapter shows the applicability of the THz-FD technique to characterise tablets and quantify changes in tablet density/porosity. Section 5.1 presents the measurement results of effective refractive index for the first formulation, and its correlation with the tablet density. Section 5.2 presents the measurement results of the effective refractive index for the second formulation, its correlation with the design factors, and the translation of effective refractive index to tablet porosity.

5.1 Tablet density characterisation

Here, we extract the effective refractive index of the tablets in the first formulation (section 3.1), using the one-path transmission method (section 4.2.2). The effective refractive index was extracted from the measured scattering parameters. We used the phase shifts of S_{21} across frequency to obtain the real part of the effective refractive index of the tablets, using equation 4.5. Fig. 5.1.a shows the real part of the extracted effective refractive index versus frequency for MCC tablets of different compaction forces. As can be observed, increasing the compaction force resulted in higher effective refractive index,

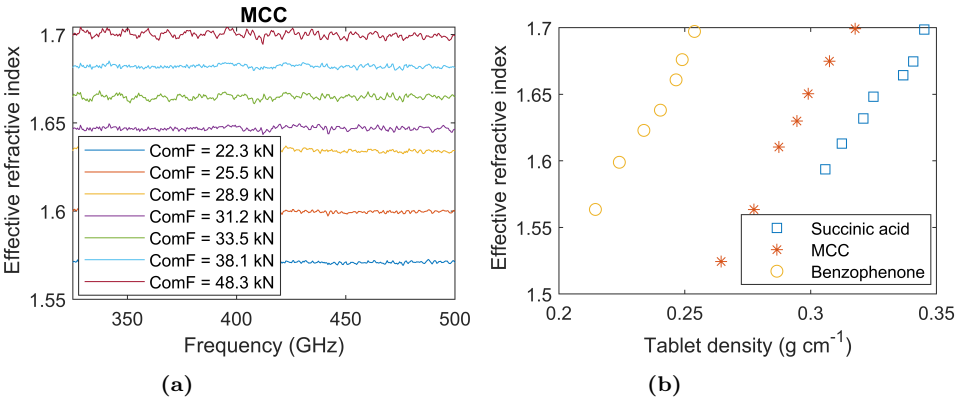

Figure 5.1: a) Effective refractive index versus frequency for MCC, for different compaction forces. Higher compaction force increases the effective permittivity. b) Effective refractive index versus tablet density, for Benzophenone, MCC, and Succinic acid. For a specific effective refractive index, the Benzophenone tablets show the lowest tablet density, followed by MCC and Succinic acid tablets, respectively.

as air voids in between particles were removed, which led to higher tablet density. Fig. 5.1.b shows the effective refractive index versus manually measured tablet density, for each set of tablets at a fixed frequency point, 420 GHz. The results verify the sensitivity of the terahertz waves to the change of the effective refractive index. For a specific tablet density, the Benzophenone tablets showed the highest effective refractive index, followed by MCC and Succinic acid tablets, respectively. Moreover, a linear correlation between effective refractive index and tablet density was observed.

5.2 Tablet porosity characterisation

5.2.1 Effective refractive index versus frequency

Here, we extract the effective refractive index of the tablets in the second formulation (section 3.2), using the multi-reflection method (section 4.2.1). We used the real part of the effective refractive index, n_s, obtained from the phase of the measured relative transmission coefficients to study the properties

of the tablets. Fig. 5.2.a shows the comparison of the phase of the measured relative transmission with that of the model presented in equation 4.1 for three tablets with the experiment number 2 in table 3.4. These tablets have the same design factors (API and filler particle size, and API concentration), but three different compaction forces, F_1= 8 kN, F_2= 12 kN, F_3= 16 kN. The good agreement between the measurements and the model validates the extraction method.

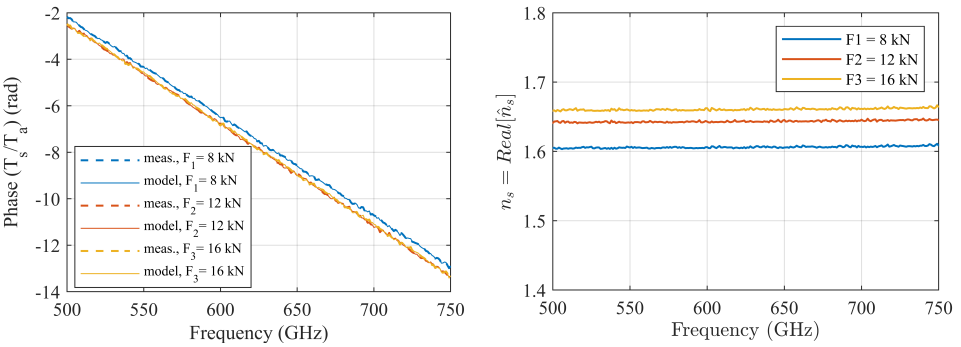

Figure 5.2: a) Phase of relative transmission for tablets (experiment number 2 in table 3.4) with three different compaction forces, F_1= 8 kN, F_2= 12 kN, F_3= 16 kN, showing good agreement between model and measurement data b) Real part of effective refractive index over frequency. A higher compaction force increased the effective refractive index.

Fig. 5.2.b shows the extracted effective refractive index of the three tablets across frequency. As observed earlier, a higher compaction force increased the effective refractive index, because of the reduced air voids in between tablet particles, leading to higher tablet density and lower porosity. The minor oscillations observed in n_s are due to the standing waves within the measurement set-up and the fact that we used the measured tablet thickness and not the effective tablet length, which in practice can be different due to the non-ideal beam properties and/or thickness and density inhomogeneities across the tablets. Fig. 5.3 shows the computed tomography scan of the tablet with experiment number 3 in table 3.4. It can be seen that tablet density is higher at the center of the tablet, and the thickness is not homogenous at the

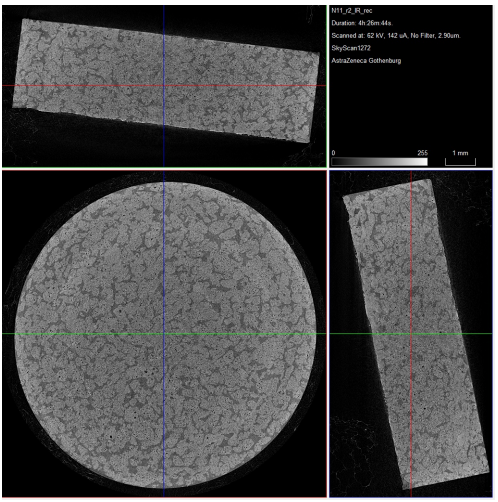

Figure 5.3: Computed tomography scan of the tablet with experiment number 3 in table 3.4 , showing the thickness/density inhomogenities across the tablet.

top and bottom surface, which will affect the effective electrical path. It was observed in Fig. 5.2.b that n_s is frequency independent. Hence, the mean value of the effective refractive index across the frequency band was chosen for data analysis.

5.2.2 Effective refractive index versus design factors

In this section, we examined the sensitivity of the THz-FD measurements to the variation of the design factors, (API and filler particle size, API concentration, and compaction force), by studying the measured effective refractive index of different tablet sets.

We used the design of the experiments [51] for evaluating the effective refractive index based on the design factors. A multi-linear regression model was applied with the effective refractive index as the response and the design factors as the independant variables, describing the contribution of each design factor. The statistical tool used for this purpose was MODDE 12 [52], and the obtained model is given as in equation 5.1:

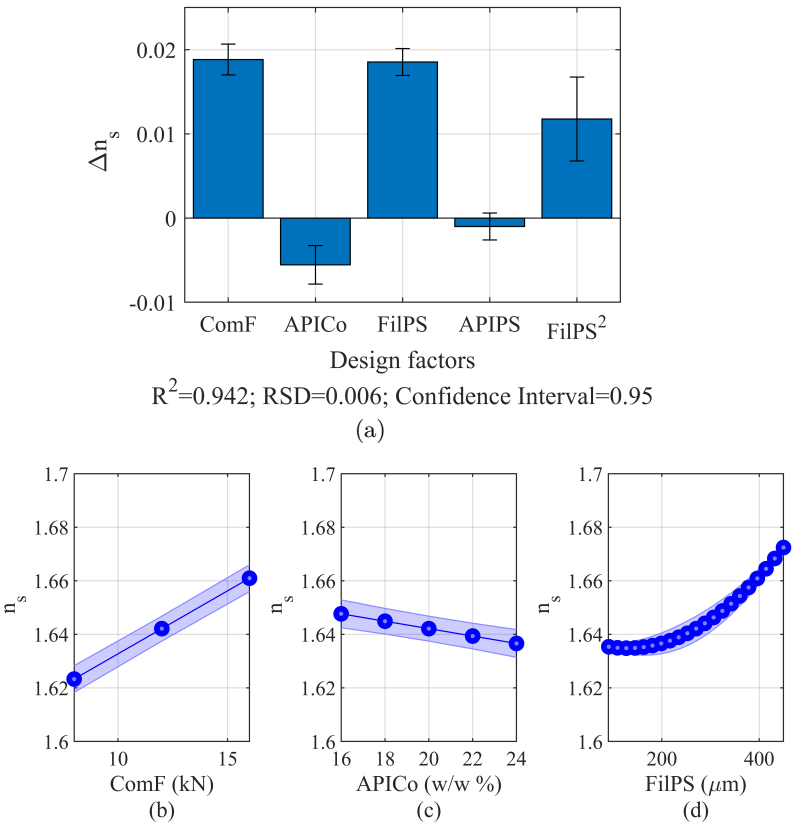

Figure 5.4: a) The change in n_s with respect to the design factors, when a factor varies from its average to high value, having the other factors at their averages. Compaction force is shown as ComF, filler particle size as FilPS, API particle size as APIPS, and API concentration as APICo. b-d) The variation of n_s with respect to the design factors. Plots are created using the multi-linear regression model in equation 5.1. In each plot, the line shows n_s and the shadowed area shows the standard deviation.

$$n_s = \beta_0 + \beta_1 x_1 + \beta_2 x_2 + \beta_3 x_3 + \beta_{33} x_3^2 + \hat{e}, \tag{5.1}$$

where x_1 is the compaction force, x_2 is the API concentration, x_3 is the filler particle size, and $\hat{e}$ is the error in the model. β_0 is the average value of n_s, and $\beta_i, i = 1, 2, 3$ are the coefficients, showing the impact of each design factor on the response.

Fig. 5.4.a shows the centered and scaled coefficients of the design factors, which are normalised and scaled to have a mean of zero and a range of two. Error bars show the uncertainty in Δn_s from each design factor. It was observed that the filler particle size, FilPS, had a larger impact than API particle size, APIPS, due to having filler as the dominant portion of the tablets. Besides that, the compaction force, ComF, had a larger effect than the API concentration, APICo, because the interval chosen for the compaction force is larger in size compared to that of the API concentration. Figs. 5.4 (b-d) show the variation of n_s with respect to each design factor, using the multi-linear regression model presented in equation 5.1. It was observed that higher compaction force results in higher effective refractive index due to removing the air voids between particles (Fig. 5.4.b), and increasing API concentration lowers the effective refractive index due to the fact that the refractive index of Ibuprofen is lower than Mannitol (Fig. 5.4.c). We also observed that larger particles are more prone to fragmentation and consolidation of the fragmented particles [53], leading to increased effective refractive index (Fig. 5.4.d). Scanning electron microscopy (SEM) (Zeiss Supra 55) photographs of the cross-section of one tablet (experiment number 3 in table 3.4) were taken for investigating the fragmentation of the particles. As can be seen in Fig. 5.5, the results showed a particle size reduction down to around 10 μm, which verified the fragmentation deformation behavior of Mannitol and Ibuprofen.

5.2.3 THz porosity versus design factors

In this section, we show the correlation between tablet density/porosity and the extracted effective refractive index from terahertz measurements, using the linear approximation described in Sec. 4.3. Later, we show the quantified THz porosity and its variation with respect to the design factors. Fig. 5.6.a shows the linear correlation between the measured effective refractive index and tablet density estimated from mass and volume measurements of the

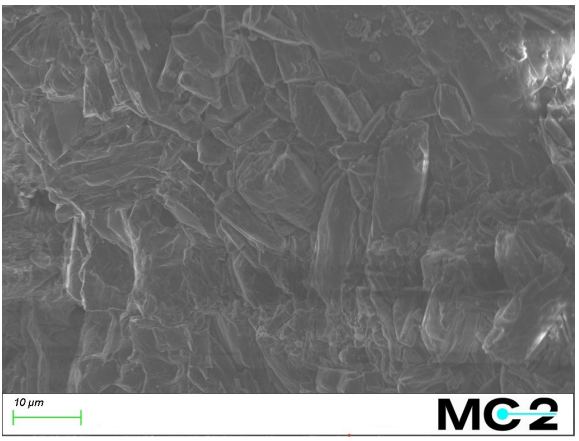

Figure 5.5: Scanning electron microscopy of cross-section of tablet (experiment number 3 in table 3.4). The fragmentation of particles while tableting process is clearly seen in this picture.

samples, which validates the assumed linear approximation. Fig. 5.6.b shows the relationship between THz porosity and the effective refractive index of the tablets, obtained by equation 4.9. The refractive index of the solid phase of the tablets for each API concentration, corresponding to zero porosity, can be estimated from the intercept with THz porosity equaling zero.

After the extraction of the THz porosity, we studied the effect of the design factors on the porosity, using the multi-linear regression method explained in section 5.2.2, having the THz porosity as the response of the system. Fig. 5.7.a shows that increasing the compaction force lowers porosity, which is in agreement with the fact that higher compaction force reduces the air voids in between particles and results in lower porosity. Fig. 5.7.b shows the reduction of the THz porosity with increasing the API concentration. It is observed in this plot that THz-FD technique is sensitive to the small variation of the API concentration from 16% to 24% [54]. The effect of filler particle size on porosity is shown in Fig. 5.7.c. It is observed that increasing the particle size of the filler first results in a slight increase in the porosity for filler particle size smaller than 150 μm and then a decrease in the porosity for larger particles. This behaviour can be explained by fragmentation behaviour of Mannitol [55] and Ibuprofen [56] under compaction force during the tableting process, and

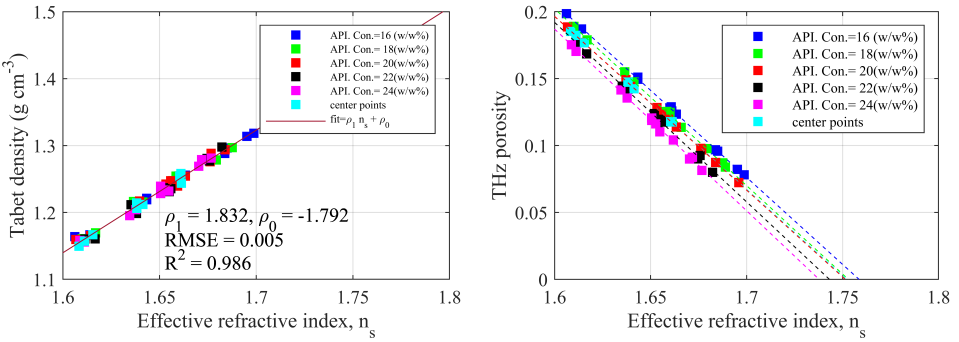

Figure 5.6: a) Correlation between the effective refractive index and tablet density. A linear relationship between the effective refractive index, n_s, and tablet density was observed. b) correlation between THz porosity and effective refractive index.

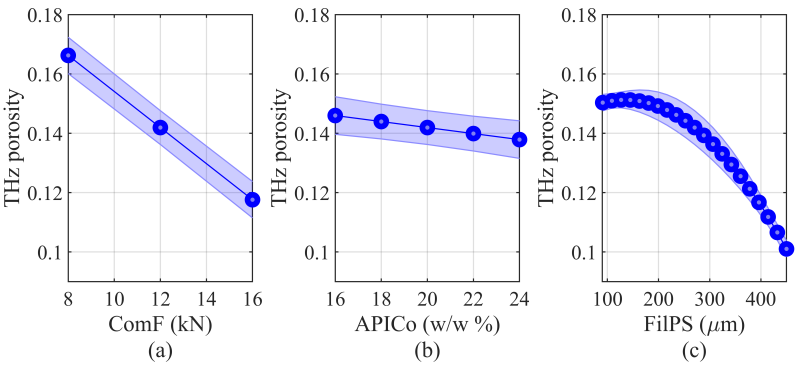

Figure 5.7: The variation of the THz porosity with respect to the design factors, a) compaction force, b) API concentration, and c) filler particle size. The plots were created using a multi-linear regression model similar to the equation 5.1. In each plot, the line shows the THz porosity and the shadowed area shows the standard deviation.

the fact that there is a greater tendency for the larger particles to fragment under high compression pressure [53]. After the fragmentation, the particles consolidate and pack together, which results in lower porosity.

CHAPTER 6

Concluding remarks and future work

Continuous manufacturing in the pharmaceutical industry demands fast, non-contact, and non-destructive techniques for the assessment of the physical properties of tablets. Although various reliable methods have been developed for this purpose, they suffer from limitations like being slow and destructive, scattering effects, low penetration depth through tablets, and bulky measurement set-up. These limitations restrict their implementation in the production for real-time measurements. In this thesis, we proposed THz-FD technique based on all-electronic solutions to address the mentioned limitation. We focused on the inspection of tablet density and porosity, which may play a crucial role in the tablet performance in the body. We studied the variation of tablet density and porosity with respect to the design factors, including compaction force, filler and API particle size, and API concentration. A VNA, frequency extenders, and quasi-optical components were used to measure the scattering parameters of tablets in transmission mode in the THz frequency range. Then, the effective refractive index of tablets was extracted and translated to tablet density and later porosity. It was observed that terahertz waves were highly sensitive to the variation of the design factors and compaction force and filler particle size showed to have the major impact on porosity for these sets of

training tablets. Moreover, it was demonstrated that THz waves can detect and quantify the minute changes in the tablet density and porosity with the variation of the design factors.

We used the relative transmission coefficients for the extraction of the complex effective refractive index. The real part of $\hat{n}_s$ was used for the characterisation of tablet porosity. The imaginary part, which was not used in this thesis, would be advantageous for example for studying the moisture content of the tablets. In our results, we observed a small uncertainty in the effective refractive index due to the inhomogeneties in tablet thickness. The precision of the extraction method can be improved by using both the reflection and transmission coefficients, and finding the effective thickness of tablets.

Because of the high-speed measurements in the THz-FD technique, this technique could be used for measuring the density of the flowing powders at an earlier stage of the production line.

High frequency resolution and dynamic range are benefits of the THz-FD technique. Pharmaceutical powders usually show absorption peaks at above 1 THz. The high frequency resolution and dynamic range of the THz-FD technique can be exploited in order to resolve the absorption peaks.

In the long term, the miniaturisation capabilities of the electronic sources and receivers enable further development for miniaturised porosity measurement systems and make the THz-FD technique promising for in-situ tablet sensing.

CHAPTER 7

Summary of appended papers

Paper A

Non-Destructive Characterization of Pharmaceutical Tablets Using Terahertz Frequency Domain Spectroscopy

In this paper, terahertz frequency domain spectroscopy (THz-FDS) in transmission mode is used to extract the effective permittivity of tablets at 325-500 GHz. We studied the sensitivity of THz waves to the change of dielectric constant, and the correlation between effective permittivity and tablet density. Three sets of training tablets, Microcrystalline cellulose (MCC), Benzophenone, and Succinic acid, which have different dielectric constants, were studied. In each set, various compaction forces were applied during the tablet compression to produce tablets with different tablet density and consequently porosity. The results showed that THz waves were sensitive to the change of the effective refractive index. Moreover, a linear correlation between effective permittivity and tablet density was observed.
My contribution: I designed the experiments, performed the measurements, analysed the data, and with the feedback from my co-authors wrote the paper.

Paper B

Small Variation of Active Pharmaceutical Ingredient Concentration Can Be Observed with THz Frequency Domain Spectroscopy

In this paper, we studied the sensitivity of THz-FD technique to the variations of the compositions of the tablets. A quasi-optical set-up with four off-axis parabolic mirrors was used to measure the scattering parameters of tablets and extract the effective refractive index in the frequency range of 500-750 GHz. We increased the concentration of the active pharmaceutical ingredient from 16% to 24%. It was observed that a small variation in API concentration could be detected by terahertz measurements and accurate extraction of the effective refractive index.
My contribution: I designed the experiments, performed the measurements, analysed the data, and with the feedback from my co-authors wrote the paper.

Paper C

Terahertz Frequency Domain Sensing for Fast Porosity Measurement of Pharmaceutical Tablets

In this paper, the THz-FD technique was explored as a fast, non-destructive, and sensitive technique for porosity measurement of pharmaceutical tablets. We studied a sample set of 69 tablets with the design factors, such as particle size of the active pharmaceutical ingredient, particle size of the filler, API concentration, and compaction force. The signal transmitted through each tablet was measured across the frequency range 500-750 GHz, using a vector network analyzer combined with a quasi-optical set-up consisting of four off-axis parabolic mirrors to guide and focus the beam. We first extracted the effective refractive index of each tablet from the measured complex transmission coefficients and then translated it to porosity, using an empirical linear relation between effective refractive index and tablet density. The results show that the THz-FD technique was highly sensitive to the variations of the design factors, showing that filler particle size and compaction force had a significant impact on the effective refractive index of the tablets and, consequently, on porosity. Moreover, a fragmentation behaviour of particles was observed

by THz porosity measurements and was verified with scanning electron microscopy of the cross-section of tablets.
My contribution: I designed the experiments, performed the measurements, analysed the data, and with the feedback from my co-authors wrote the paper.

References

[1] T. Freeman, *An introduction to powders*, 2014.

[2] M. Baumann, T. S. Moody, M. Smyth, and S. Wharry, *A Perspective on Continuous Flow Chemistry in the Pharmaceutical Industry*, 2020. DOI: 10.1021/acs.oprd.9b00524.

[3] P. Bawuah, N. Tan, S. N. A. Tweneboah, T. Ervasti, J. Axel Zeitler, J. Ketolainen, and K. E. Peiponen, "Terahertz study on porosity and mass fraction of active pharmaceutical ingredient of pharmaceutical tablets," *European Journal of Pharmaceutics and Biopharmaceutics*, vol. 105, pp. 122–133, 2016. DOI: 10.1016/j.ejpb.2016.06.007.

[4] T. Ervasti, P. Silfsten, J. Ketolainen, and K. E. Peiponen, "A study on the resolution of a terahertz spectrometer for the assessment of the porosity of pharmaceutical tablets," *Applied Spectroscopy*, vol. 66, no. 3, pp. 319–323, 2012. DOI: 10.1366/11-06315.

[5] S. Westermarck, A. M. Juppo, K. Koiranen, and J. Yliruusi, "Mercury porosimetry of pharmaceutical powders and granules," *Journal of Porous Materials*, vol. 5, no. 1, pp. 77–86, 1998. DOI: 10.1023/A:1009630015598.

[6] D. Markl, P. Wang, C. Ridgway, A. P. Karttunen, M. Chakraborty, P. Bawuah, P. Pääkkönen, P. Gane, J. Ketolainen, K. E. Peiponen, and J. A. Zeitler, "Characterization of the Pore Structure of Functionalized Calcium Carbonate Tablets by Terahertz Time-Domain Spectroscopy and X-Ray Computed Microtomography," *Journal of Pharmaceutical*

Sciences, vol. 106, no. 6, pp. 1586–1595, 2017. DOI: 10.1016/j.xphs.2017.02.028.

[7] P. Bawuah and J. A. Zeitler, *Advances in terahertz time-domain spectroscopy of pharmaceutical solids: A review*, Jun. 2021. DOI: 10.1016/j.trac.2021.116272.

[8] M. Sjöholm, G. Somesfalean, J. Alnis, S. Andersson-Engels, and S. Svanberg, "Analysis of gas dispersed in scattering media," *Optics Letters*, vol. 26, no. 1, p. 16, 2001. DOI: 10.1364/ol.26.000016.

[9] T. Svensson, L. Persson, M. Andersson, S. Svanberg, S. Andersson-Engels, J. Johansson, and S. Folestad, "Noninvasive characterization of pharmaceutical solids by diode laser oxygen spectroscopy," *Applied Spectroscopy*, vol. 61, no. 7, pp. 784–786, 2007. DOI: 10.1366/000370207781393262.

[10] J. Johansson, A. Sparén, H. Wikström, P. Tajarobi, R. Koch, P. Lundin, A. Långberg, M. Sebesta, and M. Lewander Xu, "Optical porosimetry by gas in scattering media absorption spectroscopy (GASMAS) applied to roller compaction ribbons," *International Journal of Pharmaceutics*, vol. 592, no. 2020, 2021. DOI: 10.1016/j.ijpharm.2020.120056.

[11] M. Claybourn, H. Yang, L. Gradinarsky, J. Johansson, and S. Folestad, "Terahertz Spectroscopy for Pharmaceutical Applications," in *Handbook of Vibrational Spectroscopy*, 2007. DOI: 10.1002/9780470027325.s8914.

[12] X. Lu, H. Sun, T. Chang, J. Zhang, and H. L. Cui, "Terahertz detection of porosity and porous microstructure in pharmaceutical tablets: A review," *International Journal of Pharmaceutics*, vol. 591, no. October, p. 120 006, 2020. DOI: 10.1016/j.ijpharm.2020.120006.

[13] M. Juuti, H. Tuononen, T. Prykäri, V. Kontturi, M. Kuosmanen, E. Alarousu, J. Ketolainen, R. Myllylä, and K. E. Peiponen, "Optical and terahertz measurement techniques for flat-faced pharmaceutical tablets: A case study of gloss, surface roughness and bulk properties of starch acetate tablets," *Measurement Science and Technology*, vol. 20, no. 1, 2009. DOI: 10.1088/0957-0233/20/1/015301.

[14] P. Bawuah, A. Pierotic Mendia, P. Silfsten, P. Pääkkönen, T. Ervasti, J. Ketolainen, J. A. Zeitler, and K. E. Peiponen, "Detection of porosity of pharmaceutical compacts by terahertz radiation transmission and light reflection measurement techniques," *International Journal of Pharmaceutics*, vol. 465, no. 1-2, pp. 70–76, 2014. DOI: 10.1016/j.ijpharm.2014.02.011.

[15] M. Naftaly, I. Tikhomirov, P. Hou, and D. Markl, "Measuring open porosity of porous materials using thz-tds and an index-matching medium," *Sensors (Switzerland)*, vol. 20, no. 11, 2020. DOI: 10.3390/s20113120.

[16] A. L. Skelbæk-Pedersen, M. Anuschek, T. K. Vilhelmsen, J. Rantanen, and J. A. Zeitler, "Non-destructive quantification of fragmentation within tablets after compression from scattering analysis of terahertz transmission measurements," *International Journal of Pharmaceutics*, vol. 588, Oct. 2020. DOI: 10.1016/j.ijpharm.2020.119769.

[17] S. Stranzinger, E. Faulhammer, J. Li, R. Dong, J. G. Khinast, J. A. Zeitler, and D. Markl, "Measuring bulk density variations in a moving powder bed via terahertz in-line sensing," *Powder Technology*, vol. 344, pp. 152–160, 2019. DOI: 10.1016/j.powtec.2018.11.106.

[18] P. F. Neumaier, H. Richter, J. Stake, H. Zhao, A.-Y. Tang, V. Drakinskiy, P. Sobis, A. Emrich, A. Hülsmann, T. K. Johansen, T. Bryllert, J. Hanning, V. Krozer, and H.-W. Hübers, "Molecular spectroscopy with a compact 557-GHz heterodyne receiver," *IEEE Transactions on Terahertz Science and Technology*, vol. 4, no. 4, 2014. DOI: 10.1109/TTHZ.2014.2326554.

[19] R. Dahlbäck, T. Rubaek, M. Persson, and J. Stake, "A system for THz imaging of low-contrast targets using the born approximation," *IEEE Transactions on Terahertz Science and Technology*, vol. 2, no. 3, 2012. DOI: 10.1109/TTHZ.2012.2189900.

[20] K. Sengupta, T. Nagatsuma, and D. M. Mittleman, "Terahertz integrated electronic and hybrid electronic–photonic systems," *Nature Electronics*, vol. 1, no. 12, 2018. DOI: 10.1038/s41928-018-0173-2.

[21] P. Hillger, J. Grzyb, R. Jain, and U. R. Pfeiffer, "Terahertz Imaging and Sensing Applications With Silicon-Based Technologies," *IEEE Transactions on Terahertz Science and Technology*, vol. 9, no. 1, 2019. DOI: 10.1109/TTHZ.2018.2884852.

[22] A. Moradi, M. Lindsjo, J. Stake, S. Folestad, and H. Rodilla, "Non-Destructive Characterization of Pharmaceutical Tablets Using Terahertz Frequency Domain Spectroscopy," *International Conference on Infrared, Millimeter, and Terahertz Waves, IRMMW-THz*, vol. 2019-Septe, pp. 3–4, 2019. DOI: 10.1109/IRMMW-THz.2019.8874004.

[23] M. Delalonde and T. Ruiz, "Dissolution of pharmaceutical tablets: The influence of penetration and drainage of interstitial fluids," *Chemical Engineering and Processing: Process Intensification*, vol. 47, no. 3, 2008, ISSN: 02552701. DOI: 10.1016/j.cep.2007.01.003.

[24] J. Pajander, O. Korhonen, M. Laamanen, E. L. Ryynänen, I. Grimsey, B. Van Veen, and J. Ketolainen, "Effect of formulation parameters and drug-polymer interactions on drug release from starch acetate matrix tablets," *Journal of Pharmaceutical Sciences*, vol. 98, no. 10, 2009, ISSN: 15206017. DOI: 10.1002/jps.21689.

[25] P. Wray, K. L. Chan, J. Kimber, and S. G. Kazarian, "Compaction of pharmaceutical tablets with different polymer matrices studied by FTIR imaging and X-ray microtomography," *Journal of Pharmaceutical Sciences*, vol. 97, no. 10, 2008, ISSN: 15206017. DOI: 10.1002/jps.21309.

[26] I. Akseli, S. Iyer, H. P. Lee, and A. M. Cuitiño, "A quantitative correlation of the effect of density distributions in roller-compacted ribbons on the mechanical properties of tablets using ultrasonics and X-ray tomography," *AAPS PharmSciTech*, vol. 12, no. 3, 2011, ISSN: 15309932. DOI: 10.1208/s12249-011-9640-z.

[27] R. C. Lyon, D. S. Lester, E. N. Lewis, E. Lee, L. X. Yu, E. H. Jefferson, and A. S. Hussain, "Near-infrared spectral imaging for quality assurance of pharmaceutical products: Analysis of tablets to assess powder blend homogeneity," *AAPS PharmSciTech*, vol. 3, no. 3, 2002, ISSN: 15309932. DOI: 10.1007/BF02830615.

[28] M. Khorasani, J. M. Amigo, C. C. Sun, P. Bertelsen, and J. Rantanen, "Near-infrared chemical imaging (NIR-CI) as a process monitoring solution for a production line of roll compaction and tableting," *European Journal of Pharmaceutics and Biopharmaceutics*, vol. 93, 2015, ISSN: 18733441. DOI: 10.1016/j.ejpb.2015.04.008.

[29] H. Lim, V. S. Dave, L. Kidder, E. Neil Lewis, R. Fahmy, and S. W. Hoag, "Assessment of the critical factors affecting the porosity of roller compacted ribbons and the feasibility of using NIR chemical imaging to evaluate the porosity distribution," *International Journal of Pharmaceutics*, vol. 410, no. 1-2, 2011, ISSN: 03785173. DOI: 10.1016/j.ijpharm.2011.02.028.

[30] A. V. Zinchuk, M. P. Mullarney, and B. C. Hancock, "Simulation of roller compaction using a laboratory scale compaction simulator," *International Journal of Pharmaceutics*, vol. 269, no. 2, 2004, ISSN: 03785173. DOI: 10.1016/j.ijpharm.2003.09.034.

[31] P. Bawuah, "Terahertz time-domain study on selected parameters of pharmaceutical tablets using effective medium approximations," Ph.D. dissertation, Itä-Suomen yliopisto, 2016.

[32] J. L. Hesler, Y. Duan, B. Foley, and T. W. Crowe, "THz vector network analyzer measurements and calibration," in *21st International Symposium on Space Terahertz Technology 2010, ISSTT 2010*, 2010.

[33] D. K. George, A. Charkhesht, and N. Q. Vinh, "New terahertz dielectric spectroscopy for the study of aqueous solutions," *Review of Scientific Instruments*, vol. 86, no. 12, 2015, ISSN: 10897623. DOI: 10.1063/1.4936986.

[34] D. Pozar, *Microwave Engineering Fourth Edition*. 2005. DOI: TK7876.P692011.

[35] R. Marks and D. Williams, "A general waveguide circuit theory," *Journal of Research of the National Institute of Standards and Technology*, vol. 97, no. 5, 1992, ISSN: 1044-677X. DOI: 10.6028/jres.097.024.

[36] "XII. Colours in metal glasses and in metallic films," *Philosophical Transactions of the Royal Society of London. Series A, Containing Papers of a Mathematical or Physical Character*, vol. 203, no. 359-371, 1904, ISSN: 0264-3952. DOI: 10.1098/rsta.1904.0024.

[37] M. S. Kadiri and A. Michrafy, "The effect of punch's shape on die compaction of pharmaceutical powders," *Powder Technology*, vol. 239, 2013, ISSN: 00325910. DOI: 10.1016/j.powtec.2013.02.022.

[38] G. Thoorens, F. Krier, B. Leclercq, B. Carlin, and B. Evrard, *Microcrystalline cellulose, a direct compression binder in a quality by design environment - A review*, 2014. DOI: 10.1016/j.ijpharm.2014.06.055.

[39] J. Merrylin, R. Y. Kannah, J. R. Banu, and I. T. Yeom, "Production of organic acids and enzymes/biocatalysts from food waste," in *Food Waste to Valuable Resources*, 2020. DOI: 10.1016/b978-0-12-818353-3.00006-7.

[40] IARC, "IARC Monograph. Some chemicals present in industrial and consumer products, food and drinking-water.," in *IARC Scientific Publications*, 2012.

[41] K. D. Rainsford, *Ibuprofen: Pharmacology, efficacy and safety*, 2009. DOI: 10.1007/s10787-009-0016-x.

[42] L. X. Liu, I. Marziano, A. C. Bentham, J. D. Litster, E.T.White, and T. Howes, "Effect of particle properties on the flowability of ibuprofen powders," *International Journal of Pharmaceutics*, vol. 362, no. 1-2, pp. 109–117, 2008. DOI: 10.1016/j.ijpharm.2008.06.023.

[43] A. S. Narang and S. I. Badawy, *Handbook of pharmaceutical wet granulation: Theory and practice in a quality by design paradigm*. 2018. DOI: 10.1016/C2016-0-00287-5.

[44] G. Morin and L. Briens, "The effect of lubricants on powder flowability for pharmaceutical application," *AAPS PharmSciTech*, vol. 14, no. 3, 2013, ISSN: 15309932. DOI: 10.1208/s12249-013-0007-5.

[45] D. Bourreau, A. Péden, and S. Le Maguer, "A quasi-optical free-space measurement setup without time-domain gating for material characterization in the W-band," *IEEE Transactions on Instrumentation and Measurement*, vol. 55, no. 6, pp. 2022–2028, 2006. DOI: 10.1109/TIM.2006.884283.

[46] A. M. Nicolson and G. F. Ross, "Measurement of the Intrinsic Properties Of Materials by Time-Domain Techniques," *IEEE Transactions on Instrumentation and Measurement*, vol. 19, no. 4, pp. 377–382, 1970. DOI: 10.1109/TIM.1970.4313932.

[47] W. B. Weir, "Automatic Measurement of Complex Dielectric Constant and Permeability at Microwave Frequencies," *Proceedings of the IEEE*, vol. 62, no. 1, pp. 33–36, 1974. DOI: 10.1109/PROC.1974.9382.

[48] M. Mrnka, R. Appleby, and E. Saenz, "Accurate S-parameter Modeling and Material Characterization in Quasi-Optical Systems," *IEEE Transactions on Terahertz Science and Technology*, no. c, pp. 1–1, 2022. DOI: 10.1109/tthz.2021.3140201.

[49] S. Trabelsi, A. W. Kraszewski, and S. O. Nelson, "Phase-shift ambiguity in microwave dielectric properties measurements," *IEEE Transactions on Instrumentation and Measurement*, vol. 49, no. 1, 2000. DOI: 10.1109/19.836309.

[50] C. Sun, "A Novel Method for Deriving True Density of Pharmaceutical Solids Including Hydrates and Water-Containing Powders," *Journal of Pharmaceutical Sciences*, vol. 93, no. 3, pp. 646–653, 2004. DOI: 10.1002/jps.10595.

[51] Douglas C. Montgomery, *Montgomery: Design and Analysis of Experiments*, 2000.

[52] Sartorius Stedim Data Analytics, *User Guide to MODDE - Version 12*, 2017.

[53] G. Alderborn and C. Nyström, "Studies on direct compression of tablets XIV. The effect of powder fineness on the relation between tablet permeametry surface area and compaction pressure," *Powder Technology*, vol. 44, no. 1, pp. 37–42, 1985. DOI: 10.1016/0032-5910(85)85018-X.

[54] A. Moradikouchi, A. Sparen, S. Folestad, J. Stake, and H. Rodilla, "Small Variation of Active Pharmaceutical Ingredient Concentration Can Be Observed with THz Frequency Domain Spectroscopy," *2021 46th International Conference on Infrared, Millimeter and Terahertz Waves, IRMMW-THz*, pp. 1–1, 2021. DOI: 10.1109/irmmw-thz50926.2021.9567162.

[55] N. Tarlier, I. Soulairol, N. Sanchez-Ballester, G. Baylac, A. Aubert, P. Lefevre, B. Bataille, and T. Sharkawi, "Deformation behavior of crystallized mannitol during compression using a rotary tablet press simulator," *International Journal of Pharmaceutics*, vol. 547, no. 1-2, pp. 142–149, 2018. DOI: 10.1016/j.ijpharm.2018.05.026.

[56] V. N. Le, P. Leterme, A. Gayot, and M. P. Flament, "Influence of granulation and compaction on the particle size of ibuprofen-Development of a size analysis method," *International Journal of Pharmaceutics*, vol. 321, no. 1-2, pp. 72–77, 2006. DOI: 10.1016/j.ijpharm.2006.05.010.